3

Numerical Analysis of Heat and Mass Transfer in a Fin-and-Tube Air Heat Exchanger under Full and Partial Dehumidification Conditions

Riad Benelmir and Junhua Yang
University Henri Poincaré - Nancy I
France

1. Introduction

Heat exchangers are commonly used in industrial fields such as air conditioning, petrochemical and agriculture-food industries. The design and utilization of a heat exchanger should fulfill some conditions of performance, economy and space requirement. The most widely operated heat exchangers make use of fin-and-tube configuration in association with the application of heating, ventilating, air-conditioning and refrigeration systems (Khalfi & Benelmir, 2001). With regard to the fin temperature and dew point temperature of surrounding air, three situations on a fin surface can be distinguished (Lin & Jang, 2002, Benelmir *et al.*, 2009). The fin surface is fully dry if the temperature of the whole fin is higher than the air dew point temperature. It is partially wet when the air dew point temperature is lower than the fin top temperature and is higher than the fin base temperature. Finally, the fully wet surface occurs if the temperature of the whole fin is lower than the dew point temperature. A reliable determination of the fin efficiency must account for the simultaneous heat and mass transfer on the cooling surface. Many experimental, and few numerical, studies have been carried out to study the heat and mass transfer characteristics of the fin-and-tube heat exchangers under dehumidifying conditions. It was stated by Liang *et al.* (2000) that the condensation of the moist air along the fin surface causes reduction of the fin efficiency. They found also that measured fin efficiency was less than the calculated one assuming a uniform heat transfer coefficient. The calculated results of Saboya & Sparrow (1974), Chen *et al.* (2005), Chen & Hsu (2007), and Chen & Chou (2007) concluded that the heat transfer coefficient was non-uniform under dry conditions. Due to the difficulty of considering a variable sensible heat transfer coefficient (Choukairi *et al.*, 2006), this later was often assumed to be uniform by many investigators in the calculation of fin efficiency. Liang *et al.* (2000) used one-dimensional and two-dimensional models to determine the humid fin efficiency of a plate-fin-tube heat exchanger: The results obtained show comparable efficiencies with both 1-D and 2-D models. Chen (1991) analyses the fin performance under dehumidifying conditions and shows, through a 2-D model, that the humid fin efficiency was sensitive to the moist air relative humidity value. As mentioned earlier, the sensible heat transfer coefficient is often assumed uniform. Thus, the wet fin efficiency is usually determined under this assumption and by introducing a functional relation between the relative humidity and the fin temperature [Lin & Jang , 2002, Liang *et*

al., 2000, Chen, 1991, Lin *et al.*, 2001, Elmahdy & Biggs, 1983, Coney *et al.*, 1989]. The most proposed relation between "the difference of the air humidity ratio and that evaluated at the fin temperature" and "the difference of the ambient temperature and fin temperature" used a factor named the condensation factor. This later was often settled constant. Chen & Wang (2008) proposed one-dimensional and two-dimensional models based on inverse heat conduction method and in conjunction with experimental temperature data for predicting the average overall heat transfer coefficient and wet fin efficiency. In their study the sensible heat transfer coefficient, the functional relation between the relative humidity and fin temperature, and the Lewis number are considered to be unknown. Their results show that the estimated fin efficiency under partially and fully wet conditions is sensitive to the relative humidity. Lin *et al.* (2001) mentioned that the effect of the relative humidity on the fully wet fin efficiency of extended surface was very confused. This work's aims to estimate the overall heat transfer coefficient and the fin efficiency as well as the total heat rate exchanged under partially or fully wet conditions using an appropriate numerical procedure. The airflow pattern is first determined by solving the mass and momentum balance equations. The heat and mass balance equations are then solved by a finite volume method after subdividing the fin in several sub-fin regions. The effect of admission air parameters such as temperature, relative humidity and velocity as well as the fin base temperature mainly on the overall heat transfer coefficient and the fin efficiency are investigated.

2. Mathematical model

2.1 Air dehumidification in contact with a cold wall

Cooling and dehumidifying of moist air by a cold surface involves simultaneous heat and mass transfer (Fig. 1). Within the moist air flow, characterized by the mean dry temperature Ta and absolute humidity W_a, along a cold surface at a fixed temperature T_w, which is lower than the dew point temperature of the air ($T_{dew,a}$), condensation occurs on the wall. At the air-condensate interface, the saturated air is characterized by the condensate-film temperature T_c and the saturated humidity ratio $W_{S,c}$, at T_c. The total wall heat flux includes the sensible part due to convection, spent by cooling air, resulting from the temperature differences between air and condensate-film, and the latent part due to the vapor phase transition heat leading to the partially condensation of the vapor contained in the moist air.

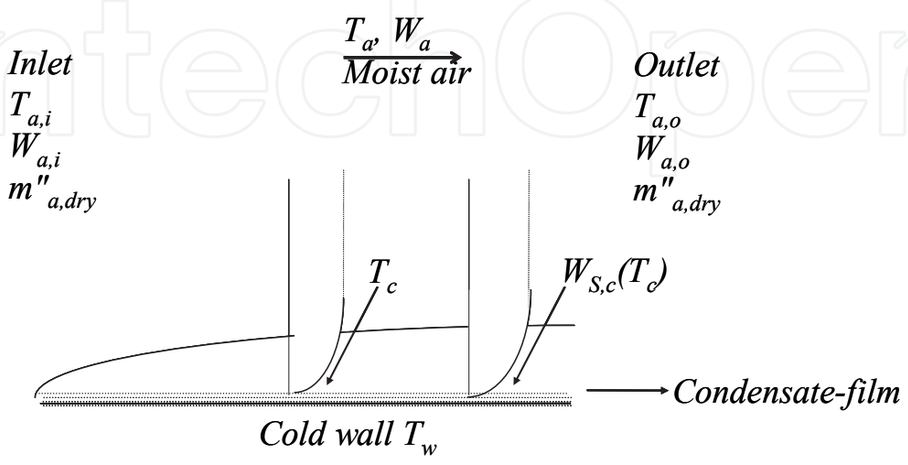

Fig. 1. Air dehumidification by a cold wall

The total heat transfer rate through the wall can be expressed as:

$$q_t'' = m_{a,dry}''\left(i_{a,i} - i_{a,o}\right) - m_c'' i_c \tag{1}$$

Where m''_c is the condensate mass flux.
The error induced by neglecting the sensible heat of the condensate $m''_c\, i_c$ is in the order of magnitude of 1.3 %. On the other hand, as stated above, the total heat flux results from both sensitive and latent heat components, thus, the following expression of total heat flux density yield:

$$q_t'' = m_{a,dry}''\left(i_{a,i} - i_{a,o}\right) = q_{sen}'' + q_l'' = \alpha_{sen,hum}\left(T_a - T_c\right) + m_c'' L_v \tag{2}$$

According to the mass transfer law, the mass flux of the condensate is expressed as:

$$m_c'' = \alpha_m\left(W_a - W_{S,c}\right) \tag{3}$$

As reported by Lin *et al.* (2001), most of the investigators applied the Chilton-Colburn analogy to set a relationship between the mass transfer coefficient and the sensitive heat transfer coefficient, hence; the following relation is reported and used in our work:

$$\alpha_m = \frac{\alpha_{sen,hum}}{Le^{2/3}.c_{p,a}} \tag{4}$$

Combining equations (2), (3), and (4), the following equation is obtained:

$$q_t'' = \alpha_{sen,hum}\left[\left(T_a - T_c\right) + \frac{Lv}{Le^{2/3}.c_{p,a}}\left(W_a - W_{S,c}\right)\right] \tag{5}$$

Moreover, the total heat flux density is related to the overall heat transfer coefficient by the following relation:

$$q_t'' = \alpha_{O,hum}\left(T_a - T_c\right) \tag{6}$$

Thus, we obtain the expression bellow for the overall heat transfer coefficient:

$$\alpha_{O,hum} = \alpha_{sen,hum}\left[1 + \frac{Lv}{Le^{2/3}.c_{p,a}}\frac{W_a - W_{S,c}}{T_a - T_c}\right] \tag{7}$$

2.2 The physical problem

The schematic diagram of the problem is shown in Fig. 2. The rectangular fins are arranged around tubes lined up or ranked in staggered rows. The refrigerant flows inside tubes and moist air streams outside. The fin temperature is considered lower than the dew point temperature of air, which draws away a condensation on the surface of the tube and the fin. This work will consider the heat and mass transfer for a representative tube and fin elementary unit.

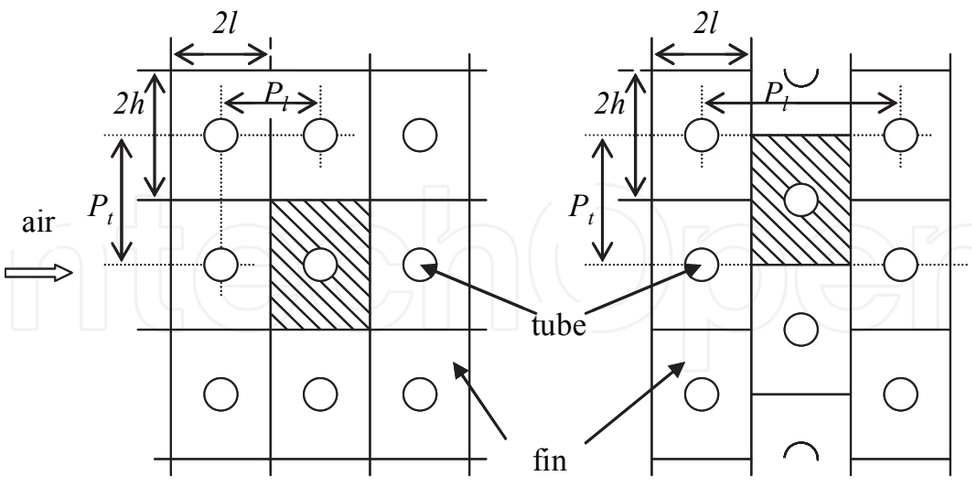

Fig. 2. Schematic of fins arranged around tubes lined up or ranked in staggered rows

The investigation of heat and mass transfer performance during the cooling of moist air through an extended surface, associated with dehumidification, should take into account: the convective heat transfer process between the air-flow and the condensate-film, the conduction inside the fin and the condensate-film, and the mass transfer process between the air-flow and the condensate-film (Fig. 3).

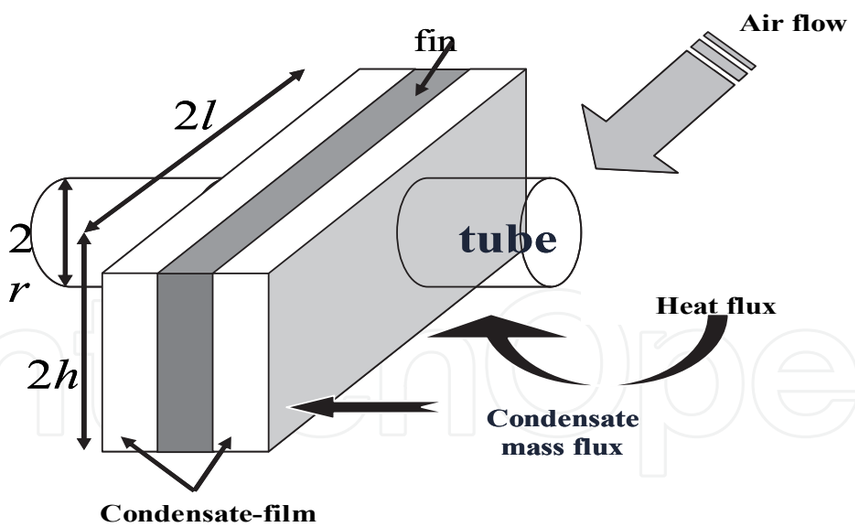

Fig. 3. Heat and mass transfer phenomenon around a fin-tube

As the fins spacing is very weak regarding the fins height and length, heat and mass transfer along with the fin plane's normal direction (z direction) is neglected. The heat flux exchanged by the fin is assumed to be identical on both faces. Hence, only one face is considered in the study of heat and mass transfer by the fin as a result of symmetry condition applied on the fin median plane. Fig. 4 shows the physical domain of the current work.

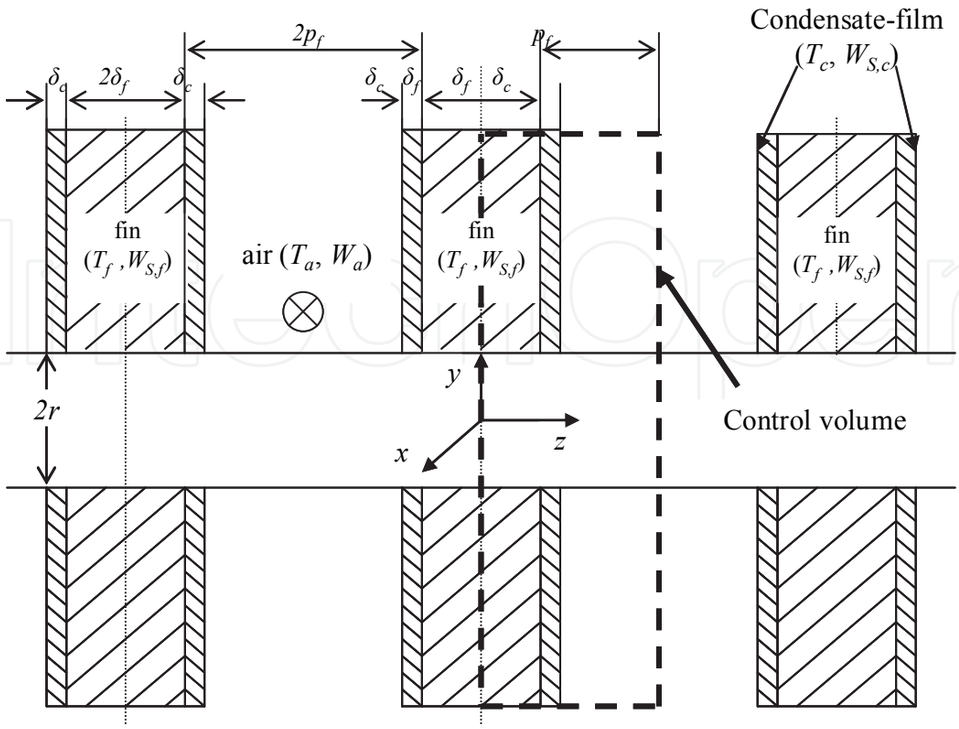

Fig. 4. Physical domain of the present work

The elementary volumes are defined as follow:

$$V_f = \delta_f dxdy \; ; \quad V_c = \delta_c dxdy \; ; \quad V_a = \left(p_f - \delta_c\right) dxdy \; ; \quad V_t = \left(p_f + \delta_f\right) dxdy$$

2.3 Governing equations

In this work, we consider the two-dimensional problem of heat transfer through the fin-surface and condensate-film and the dynamic air-stream according to the (x,y) plane (Fig. 4). The problem of the vapor mass transfer from air to the fin-tube wall occurs according to the direction z. The mathematical formulation is accomplished with respect to some basic assumptions. The air-flow is considered as incompressible and evolving in a laminar steady state. The thermo-physical properties of air, condensate-film and fin-tube are temperature dependant. On the other hand, we consider that heat transfer through the condensate-film is purely conductive and that the radiation transfer mode is always neglected. Furthermore, the condensate-film is assumed to be thin and uniform and, due to the weak thickness of the fin, the adiabatic condition is assumed at the fin-end. For convenience of heat and mass transfer analysis, the following dimensionless parameters are introduced as:

$$T_a^* = \frac{T_a - T_{f,b}}{T_{a,i} - T_{f,b}} \qquad T_f^* = \frac{T_f - T_{f,b}}{T_{a,i} - T_{f,b}} \tag{8}$$

$$W_a^* = \frac{W_a - W_{S,f,b}}{W_{a,i} - W_{S,f,b}} \qquad W_c^* = \frac{W_{S,c} - W_{S,f,b}}{W_{a,i} - W_{S,f,b}} \tag{9}$$

$$x^* = \frac{x}{r} \quad y^* = \frac{y}{r} \quad h^* = \frac{h}{r} \quad l^* = \frac{l}{r} \quad r^* = \frac{r}{r} = 1 \tag{10}$$

$$P^* = \frac{P_f}{r} \quad \delta_c^* = \frac{\delta_c}{r} \quad u_x^* = \frac{u_x}{u_i} \quad u_y^* = \frac{u_y}{u_i} \tag{11}$$

2.3.1 Continuity and momentum equations for air flow

The two-dimensional continuity and momentum equations for air-flow are:

$$\frac{\partial u_x}{\partial x} + \frac{\partial u_y}{\partial y} = 0 \tag{12}$$

$$u_x \frac{\partial u_x}{\partial x} + u_y \frac{\partial u_x}{\partial y} = \nu_a \left(\frac{\partial^2 u_x}{\partial x^2} + \frac{\partial^2 u_x}{\partial y^2} \right) \tag{13}$$

$$u_x \frac{\partial u_y}{\partial x} + u_y \frac{\partial u_y}{\partial y} = \nu_a \left(\frac{\partial^2 u_y}{\partial x^2} + \frac{\partial^2 u_y}{\partial y^2} \right) \tag{14}$$

Introducing the dimensionless variables defined above into Eqs. (12) to (14) leads to the following dimensionless equations:

$$\frac{\partial u_x^*}{\partial x^*} + \frac{\partial u_y^*}{\partial y^*} = 0 \tag{15}$$

$$u_x^* \frac{\partial u_x^*}{\partial x^*} + u_y^* \frac{\partial u_x^*}{\partial y^*} = \frac{2}{\mathrm{Re}_D} \left(\frac{\partial^2 u_x^*}{\partial x^{*2}} + \frac{\partial^2 u_x^*}{\partial y^{*2}} \right) \tag{16}$$

$$u_x^* \frac{\partial u_y^*}{\partial x^*} + u_y^* \frac{\partial u_y^*}{\partial y^*} = \frac{2}{\mathrm{Re}_D} \left(\frac{\partial^2 u_y^*}{\partial x^{*2}} + \frac{\partial^2 u_y^*}{\partial y^{*2}} \right) \tag{17}$$

Where Re_D indicates the Reynolds number based on the internal fin diameter.

$$\mathrm{Re}_D = \frac{\rho_a u_i D}{\mu_a} \tag{18}$$

The air speed at the inlet and outlet is settled uniform and parallel to the x axes, which yields to the following boundary conditions:

$$x^* = \pm l^*, \quad \forall y^*, \quad u_x^* = 1, \quad u_y^* = 0 \tag{19}$$

The upper and lower edges of the fin are subject to the following boundary conditions:

$$y^* = \pm h^*, \quad \forall x^*, \quad u_y^* = 0 \tag{20}$$

Finally, at the fin base, the non-sliding condition is used:

$$\sqrt{x^{*2}+y^{*2}}=1 \quad u_x^*=u_y^*=0 \tag{21}$$

2.3.2 Mass balance equation for vapor in air flow

The vapor flow mass balance equation in the elementary air volume, represented by Fig. 5, is expressed as follow:

$$\Delta \dot{m}_v + m_c'' dxdy = 0 \tag{22}$$

In this equation, the first term represents the vapor flow rate variation in the air volume, and the second term corresponds to the mass flow rate between the moist air and the condensate-film.

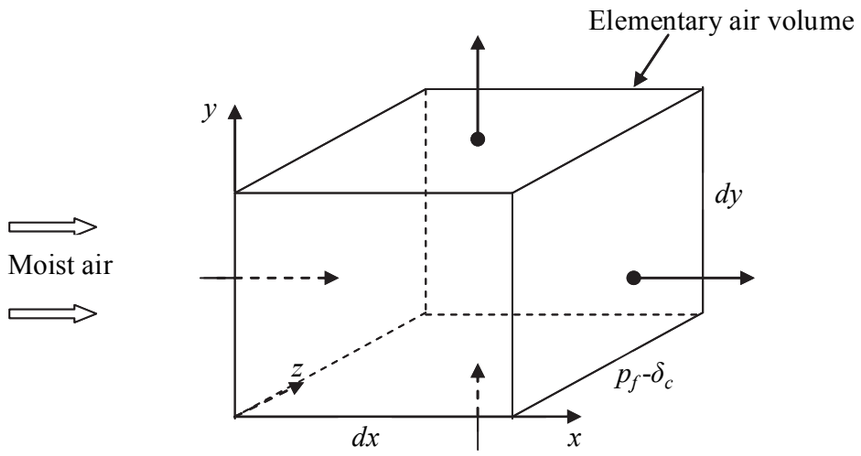

Fig. 5. Vapor flow rate variation in an elementary air volume

According to Fig. 5, the variation of the vapor mass flow is written as:

$$\Delta \dot{m}_v = \left[u_x \frac{\partial W_a}{\partial x} + u_y \frac{\partial W_a}{\partial y} \right] \rho_{a,dry} V_a \tag{23}$$

Using Eqs. (3), (22) and (23) yields to the following equation:

$$u_x \frac{\partial W_a}{\partial x} + u_y \frac{\partial W_a}{\partial y} = -\frac{\alpha_{sen,hum}}{\left(p_f - \delta_c\right).Le^{2/3}.c_{p,a}.\rho_{a,dry}} \left(W_a - W_{S,c}\right) \tag{24}$$

The dimensionless form becomes:

$$u_x^* \frac{\partial W_a^*}{\partial x^*} + u_y^* \frac{\partial W_a^*}{\partial y^*} = -\frac{\alpha_{sen,hum}}{\left(p^* - \delta_c^*\right).Le^{2/3}.c_{p,a}.u_i.\rho_{a,dry}} \left(W_a^* - W_c^*\right) \tag{25}$$

And the corresponding boundary conditions are:

$$x^* = -l^*, \quad \forall y^*, \quad W_a^* = 1$$
$$y^* = \pm h^*, \quad \forall x^*, \quad \frac{\partial W_a^*}{\partial y^*} = 0 \tag{26}$$

2.3.3 Energy balance equation for air flow

Referring to Fig. 5, the energy balance equation held the same form as Eq. (22):

$$\Delta \dot{E}_a + q_{sen}{}'' dxdy = 0 \tag{27}$$

This equation denotes that the most air sensible heat variation of the elementary volume is equilibrated by the sensible heat flow exchanged between air and the condensate-film.
The variation of the sensible heat of the elementary volume can be expressed as:

$$\Delta \dot{E}_a = c_{p,a}\left[u_x \frac{\partial T_a}{\partial x} + u_y \frac{\partial T_a}{\partial y}\right]\rho_{a,dry} V_a \tag{28}$$

Using Eq. (2) and (27), Eq. (28) leads the following form:

$$u_x \frac{\partial T_a}{\partial x} + u_y \frac{\partial T_a}{\partial y} = -\frac{\alpha_{sen,hum}}{\left(p_f - \delta_c\right).Le^{2/3}.c_{p,a}.\rho_a}\left(T_a - T_c\right) \tag{29}$$

After introducing the dimensionless variables, we get :

$$u_x^* \frac{\partial T_a^*}{\partial x^*} + u_y^* \frac{\partial T_a^*}{\partial y^*} = -\frac{\alpha_{sen,hum}}{\left(p^* - \delta_c^*\right).Le^{2/3}.c_{p,a}.u_i.\rho_a}\left(T_a^* - T_c^*\right) \tag{30}$$

The related boundary conditions are:

$$x^* = -l^*, \quad \forall y^*, \quad T_a^* = 1 \tag{31}$$

$$y^* = \pm h^*, \quad \forall x^*, \quad \frac{\partial T_a^*}{\partial y^*} = 0 \tag{32}$$

2.3.4 Energy balance equation for the condensate-film

As mentioned above, heat transfer through the condensate-film is assumed to be purely conductive. Using the fact that the temperature of the condensate-film internal surface is the same as that of the fin surface, the heat flux transferred from the condensate-film to the fin is:

$$q_t'' = \lambda_c \frac{T_c - T_f}{\delta_c} \tag{33}$$

This flux is equal to the convective heat flow transferred by air to the condensate-film, consequently, Eq. (33) can be written:

$$\alpha_{O,hum}\left(T_a - T_c\right) = \lambda_c \frac{T_c - T_f}{\delta_c} \tag{34}$$

From this equation, the condensate-film temperature is deduced:

$$T_c = T_a - \frac{T_a - T_f}{1 + \alpha_{O,hum}\dfrac{\delta_c}{\lambda_c}} \tag{35}$$

2.3.5 Mass balance equation for condensate-film

The film-wise condensation of a stationary saturated vapor on a plane vertical surface has been analyzed by Nusselt (1916) by means of some assumptions. The expression of the condensate-film thickness given by Nusselt is:

$$\delta_c = \left(\frac{4\mu_c\lambda_c\left(h - y\right)\left(T_c - T_f\right)}{gL_v\rho_c\left(\rho_c - \rho_v\right)} \right)^{1/4} \tag{36}$$

Where the subscripts c and v refer to condensate-film and water vapor, respectively.
Substituting T_c by its expression (Eq. 35) into Eq. (36) leads to the following relationship:

$$\delta_c = \left(\frac{4\mu_c\lambda_c\left(h - y\right)\left(T_a - T_f\right)}{gL_v\rho_c\left(\rho_c - \rho_v\right)} \cdot \frac{\lambda_c}{\lambda_c + \alpha_{O,hum}\delta_c} \right)^{1/4} \tag{37}$$

2.3.6 Energy balance equation for the fin surface

The energy balance equation for the fin is obtained from the heat conduction equation within the fin surface, thus, the subsequent equation is obtained:

$$\lambda_f\left[\frac{\partial^2 T_f}{\partial x^2} + \frac{\partial^2 T_f}{\partial y^2}\right] + \Delta\dot{E}_f = 0 \tag{38}$$

Where, ΔE_f is the thermal energy flow rate received by the fin elementary volume, expressed as:

$$\Delta\dot{E}_f = \frac{q_t'' dxdy}{V_f} = \frac{\alpha_{O,hum}\lambda_c}{\delta_f\left(\lambda_c + \alpha_{O,hum}\delta_C\right)}\left(T_a - T_f\right) \tag{39}$$

Combining these equations yields:

$$\left[\frac{\partial^2 T_f}{\partial x^2} + \frac{\partial^2 T_f}{\partial y^2}\right] + \frac{\alpha_{O,hum}\lambda_c}{\lambda_f\delta_f\left(\lambda_c + \alpha_{O,hum}\delta_C\right)}\left(T_a - T_f\right) = 0 \tag{40}$$

The dimensionless form of Eq. (40) is:

$$\left[\frac{\partial^2 T_f^*}{\partial x^{*2}}+\frac{\partial^2 T_f^*}{\partial y^{*2}}\right]+\frac{r^2\alpha_{O,hum}\lambda_c}{\lambda_f\delta_f\left(\lambda_c+\alpha_{O,hum}\delta_C\right)}\left(T_a^*-T_f^*\right)=0 \tag{41}$$

Using the adiabatic condition in the inlet and the outlet as well as the symmetry condition in both upper and lower, of the fin wall, the following boundary conditions holds:

$$x^*=\pm l^*,\ \forall y^*,\ \frac{\partial T_f^*}{\partial x^*}=0 \tag{42}$$

$$y^*=\pm h^*,\ \forall x^*,\ \frac{\partial T_f^*}{\partial y^*}=0 \tag{43}$$

At the fin base surface, the temperature is considered equal to that of the tube:

$$\sqrt{x^{*2}+y^{*2}}=1,\ T_f^*=0 \tag{44}$$

2.4 Solving equations

The two-dimensional model developed above is based on the following equations: the continuity and momentum equation (Eqs. 15 to 17), the mass balance equation for water vapor (Eq. 25), the energy balance equation for air stream (Eq. 30), the heat transfer equation in the fin surface (Eq. 41) and the heat and mass transfer equations for the condensate-film (Eqs. 35 and 37). In our model, the simultaneous influence of the local speed and heat transfer coefficient is considered for solving heat and mass transfer within the air flow (Eqs.25 and 30). Moreover, equation (30) uses in its expression the mass flow of moist air ($\rho_a u_i$), while in Eq. (25), the dry air mass flow is used. This allows the consideration of the effect of condensation on heat and mass transfer only once.

2.4.1 Solving continuity and momentum equations

The problem described by Eqs (15) to (17) is a classical fluid flow problem, as the flow around a cylinder. However, in our case, the fluid flows inside a rectangular channel. In order to analyze the heat and mass transfer fin performance, it is necessary to know the airflow pattern, particularly the distribution of the airflow velocities. The investigation of air velocity field has been carried out either by using the analytical approaches given by Johnson (1998) or by a numerical analysis using the finite-volume method. In the completion of this work, as the Reynolds number based on fin length is less than 2000 (laminar case) and as the air thermo-physical properties are weakly temperature dependent, except the kinetic viscosity, the following expressions of the dimensionless velocities found by Johnson (1998) are approved:

$$u_x^*=1-\frac{1}{x^{*2}+y^{*2}}+\frac{2y^{*2}}{\left(x^{*2}+y^{*2}\right)^2} \tag{45}$$

$$u_y^*=-\frac{2x^*y^*}{\left(x^{*2}+y^{*2}\right)^2} \tag{46}$$

The distributions of these velocities over the physical domain, where the half fin length and high are settled to 2.5, are shown in Fig. 6a and 6b.

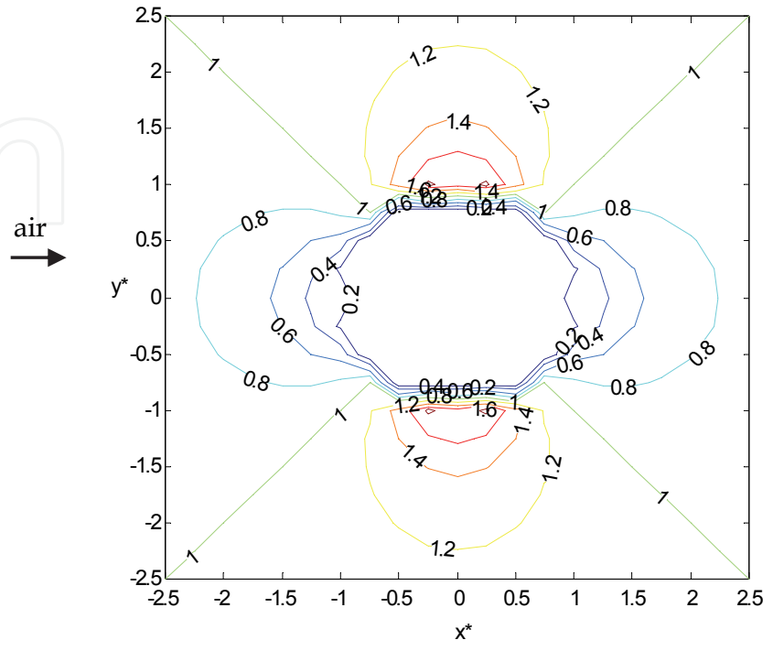

Fig. 6a. Horizontal velocity distribution

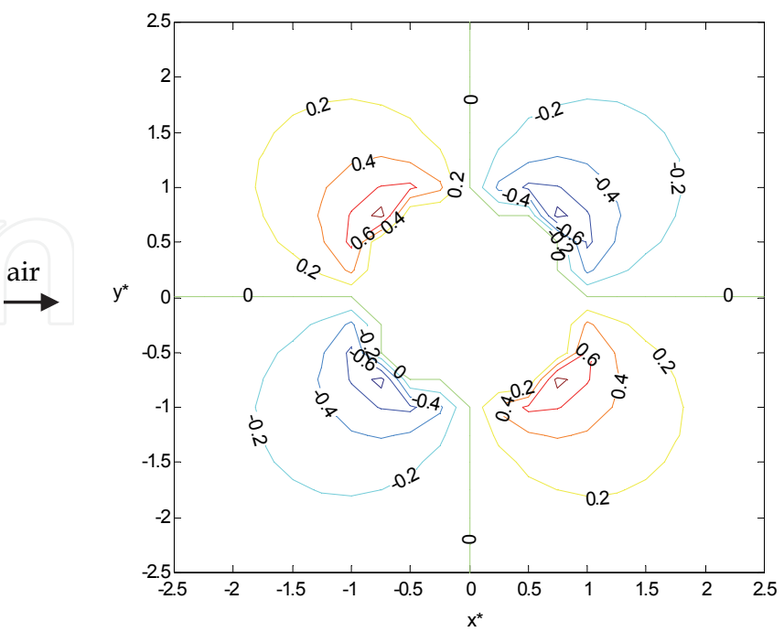

Fig. 6b. Vertical velocity distribution

As shown in Fig. 6a and 6b, the horizontal and vertical velocities fields present an apparent symmetry regarding x and y axes. The horizontal dimensionless velocity at the inlet and outlet tends towards unity, is maximal at the upper and lower fin edges and is minimal close to the tube wall as a result of the channel reduction. Likewise, the vertical dimensionless velocity is close to zero when going up the inlet and outlet or the upper and lower fin edges, and is also minimal near the tube surface.

2.4.2 Solving heat and mass transfer equations

The heat and mass transfer problem has been solved using an appropriate meshing of the calculation domain and a finite-volume discretization method. Fig. 7 illustrates the fin meshing configuration used.

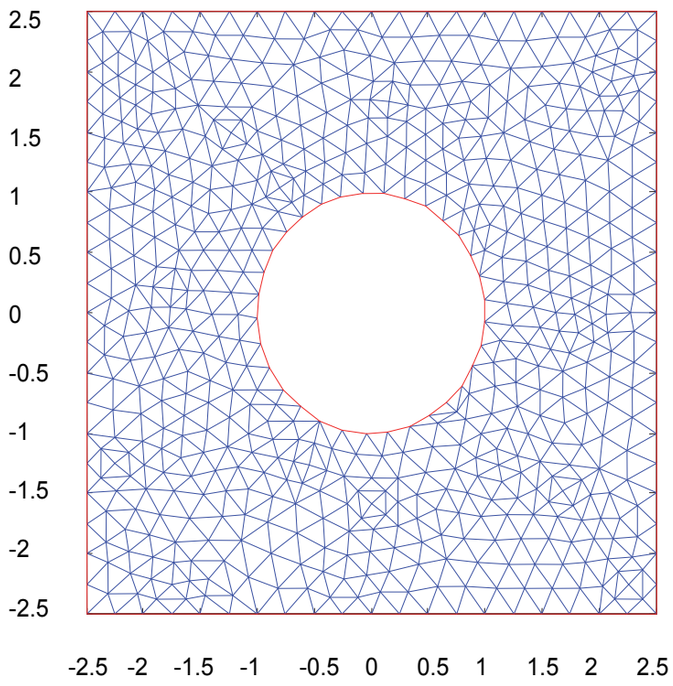

Fig. 7. Fin meshing with 627 nodes. *(h^*=2.5, l^*=2.5)*

In this work, up to 11785 nodes are used in order to take into account the effect of the mesh finesse on the process convergence and results reliability. The deviations on the calculation results of the fin efficiency with the different meshing prove to be less than 0.3 %. The numerical simulation is achieved using MATLAB simulation software. A global calculation algorithm for heat and mass transfer models is developed and presented in Fig. 8.

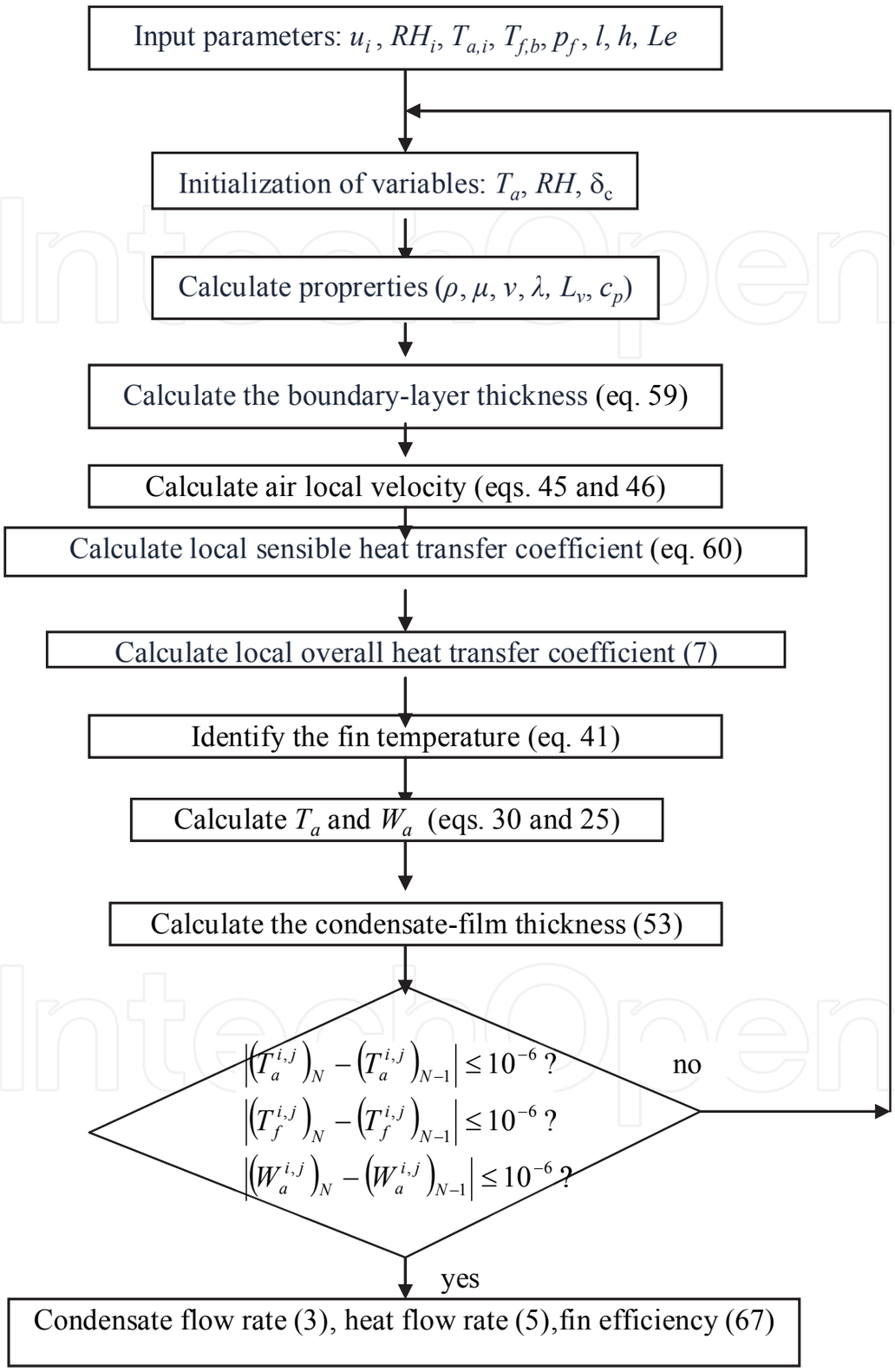

Fig. 8. The global calculation algorithm for heat and mass transfer models

2.5 Heat performance characterization

In order to evaluate the fin thermal characteristics, we need to define the heat transfer coefficients, the Colburn factor j, and the fin efficiency η_f.

2.5.1 Colburn factor

The sensible Colburn factor is expressed as:

$$j_{sen} = \frac{Nu_{sen}}{\mathrm{Re}_{Dh}.\mathrm{Pr}^{1/3}} \tag{47}$$

The Reynolds number based on the hydraulic diameter is defined as follows:

$$\mathrm{Re}_{Dh} = \frac{\rho_a u_{\max,a} D_h}{\mu_a} \tag{48}$$

where the maximal moist air velocity $u_{\max,a}$ is obtained at the contraction section of the flow :

$$u_{\max,a} = \frac{2h^*}{2h^* - 2} u_i \tag{49}$$

By definition, the hydraulic diameter is expressed as:

$$D_h = \frac{8h^* l^* p^* - 2\pi p^*}{4h^* l^* - \pi + \pi p^*} \tag{50}$$

The Nusselt and Prandtl numbers are given by:

$$Nu_{sen} = \frac{\alpha_{sen,hum}.D_h}{\lambda_a} \tag{51}$$

$$\mathrm{Pr} = \frac{\mu_a.c_{p,a}}{\lambda_a} \tag{52}$$

The Colburn factor takes into account the effect of the air speed and the fin geometry in the heat exchanger. Knowing the heat transfer coefficient, the determination of Colburn factor becomes usual.

2.5.2 Heat transfer coefficients

Regarding the physical configuration of the fin-and-tube heat exchanger, the condensate distribution over the fin-and-tube is complex. In this work, the condensate film is assumed uniformly distributed over the fin surface and the effect of the presence of the tube on the film distribution is neglected. The average condensate-film thickness is calculated as follow:

$$\overline{\delta}_c = \frac{\int_{A_t}^{A_f + A_t} \delta_c ds}{A_f} \tag{53}$$

where A_f denotes the net fin area:

$$A_f = 4lh - \pi r^2 \tag{54}$$

And A_t represents the total tube cross section:

$$A_t = \pi r^2 \tag{55}$$

The condensate-thickness δ_c is calculated using equation (37) and can be estimated iteratively. Assuming the temperature profile of the condensate-film to be linear, the heat transfer coefficient of condensation is obtained as follow:

$$\alpha_c = \frac{\lambda_c}{\delta_c} \tag{56}$$

The theory of hydrodynamic flow over a rectangular plate associated with heat and mass transfer allows us to evaluate the sensible heat transfer coefficient. In this case, a hydro-thermal boundary-layer is formed and results from a non-uniform distribution of temperatures, air velocity and water concentrations across the boundary layer (Fig.9).

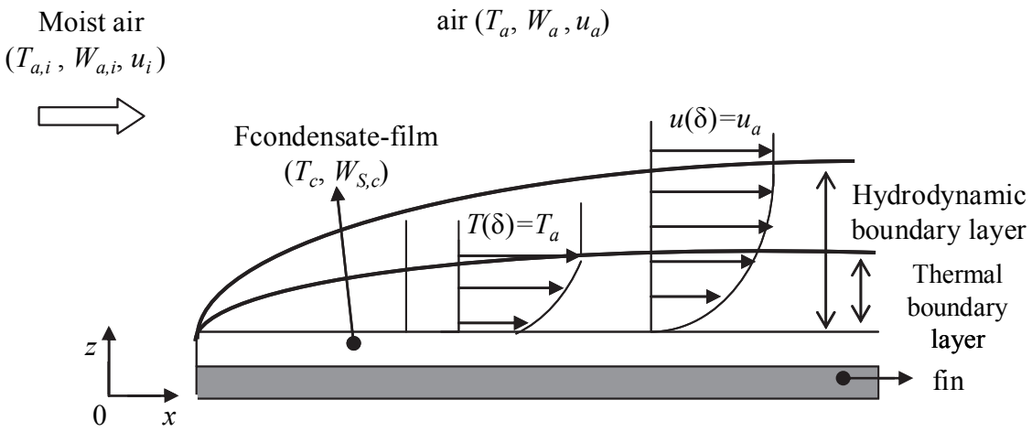

Fig. 9. Thermal and hydrodynamic boundary layer on a plate fin

According to Blasius theory, the hydraulic boundary layer thickness can be defined as follow:

$$\delta_H = \frac{5.x}{\mathrm{Re}_L^{1/2}} \quad \text{with} \quad \mathrm{Re}_L = \frac{u_a.x}{\nu_a} \tag{57}$$

where Re_L is the Reynolds number based on the longitudinal distance x.
By analogy, the thermal boundary layer thickness is associated to the hydraulic boundary layer thickness through the Prandtl number (Hsu, 1963):

$$\frac{\delta_T}{\delta_H} = \mathrm{Pr}^{-1/3} \tag{58}$$

The expression of δ_t takes the following form:

$$\delta_T = \frac{5.x}{\mathrm{Re}_L^{1/2}.\mathrm{Pr}^{1/3}} \tag{59}$$

Assuming a linear profile of temperature along within the boundary layer, the sensible heat transfer coefficient is related to the thermal boundary layer thickness by the following relation:

$$\alpha_{sen,hum} = \frac{\lambda_a}{\overline{\delta}_T} \tag{60}$$

Where, δ_t is the average thickness of the thermal boundary layer.
The overall heat transfer coefficient, estimated from equation (7), involves the sensible heat-transfer coefficient and the part due to mass transfer. The exact values of the average sensible and overall heat-transfer coefficients can be obtained by:

$$\overline{\alpha}_{sen,hum} = \frac{\int_{A_t}^{A_f+A_t} \alpha_{sen,hum} ds}{A_f} \quad \overline{\alpha}_{O,hum} = \frac{\int_{A_t}^{A_f+A_t} \alpha_{O,hum} ds}{A_f} \tag{61}$$

2.5.3 Fin efficiency

In this work, the local fin efficiency in both dry and wet conditions is estimated by the following relations:

$$\eta_{f,dry} = \frac{\alpha_{sen,dry}\left(T_a - T_f\right)}{\alpha_{sen,dry}\left(T_{a,i} - T_{f,b}\right)} = T_a^* - T_f^* \tag{62}$$

$$\eta_{f,hum} = \frac{\alpha_{sen,hum}\left(T_a - T_f\right)\left(1 + \frac{Lv}{Le^{2/3}c_{p,a}}.\frac{W_a - W_{S,f}}{T_a - T_f}\right)}{\alpha_{sen,hum}\left(T_{a,i} - T_{f,b}\right)\left(1 + \frac{Lv}{Le^{2/3}c_{p,a}}.\frac{W_{a,i} - W_{S,f,b}}{T_{a,i} - T_{f,b}}\right)} = \left(T_a^* - T_f^*\right)\frac{\left(1 + \frac{Lv}{Le^{2/3}c_{p,a}}.C\right)}{\left(1 + \frac{Lv}{Le^{2/3}c_{p,a}}.C_i\right)} \tag{63}$$

Where the condensation factors are given by:

$$C = \frac{W_a - W_{S,f}}{T_a - T_f} \tag{64}$$

$$C_i = \frac{W_{a,i} - W_{S,f,b}}{T_{a,i} - T_{f,b}} \tag{65}$$

The averages values of the fin efficiencies over the whole fin are estimated as follow:

$$\overline{\eta}_{f,dry} = \frac{\int_{A_t}^{A_f+A_t} \alpha_{sen,dry}\left(T_a^* - T_f^*\right) ds}{\int_{A_t}^{A_f+A_t} \alpha_{sen,dry} ds} \tag{66}$$

$$\bar{\eta}_{f,hum} = \frac{\int_{A_t}^{A_f+A_t} \alpha_{sen,dry}\left(T_a^* - T_f^*\right)\left(1+\frac{Lv}{Le^{2/3}c_{p,a}}.C\right)ds}{\left(1+\frac{Lv}{Le^{2/3}c_{p,a}}.C_i\right)\int_{A_t}^{A_f+A_t} \alpha_{sen,dry}ds} \tag{67}$$

3. Results and discussion

In This section, the simulation results of the heat and mass transfer characteristics during a streamline moist air through a rectangular fin-and-tube will be shown. The effect of the hydro-thermal parameters such us air dry temperature, fin base temperature, humidity, and air velocity will be analyzed. The key-parameters values for this work are selected and reported in the table 1. A central point is uncovered for the main results representations. This point corresponds to a fully wet condition problem.

Parameter	Central point values	range
Fin high, h^*	2.5	-
Fin length, l^*	2.5	-
Fin spacing, p^*	0.16	-
Inlet air speed, u_i	3 m/s	1-5 m/s
Fin base temperature, $T_{f,b}$	9 °C	1-9 °C
Inlet air dry temperature, $T_{a,i}$	27 °C	24-37 °C
Inlet air relative humidity, RH_i	50 %	20-100 %
Lewis number, Le	1	-

Table 1. Values of the parameters used in this work

3.1 The fully wet condition

Figures 10a and 10b show, respectively, the distribution of the curve-fitted air temperature inside the airflow region and that of the fin temperature for the values of the parameters indicated by the central point.

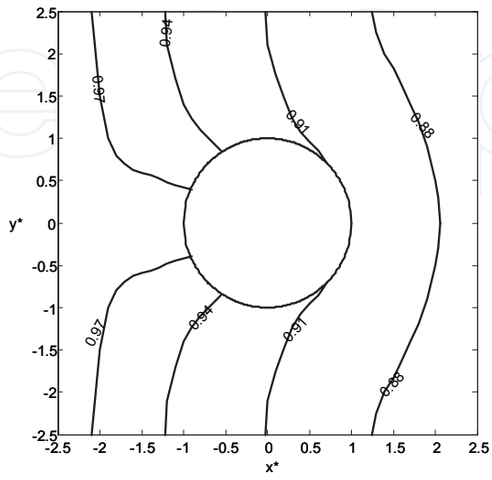

Fig. 10a. Air temperature distribution

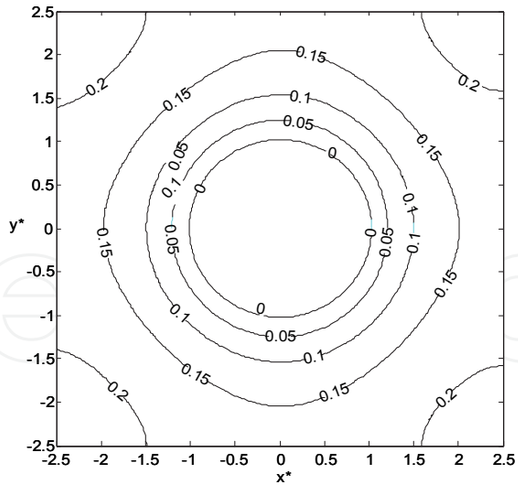

Fig. 10b. Fin temperature distribution

Initially, the air temperature is uniform (T^*_a=1) then decreases along the fin. As the fin temperature is minimal at the vicinity of the tube, air temperature gradient is more important near the tube than by the fin borders. However, at the outlet of the flow, the temperature gradient of air is weaker than at the inlet due to the reduction of the sensible heat transfer upstream the fin. The increasing of the boundary layer thickness along the fin causes a drop of the heat transfer coefficient. It is worth noting that the isothermal temperature curves are normal to the fin borders because of the symmetric boundary condition. Concerning the fin temperature T^*_f, it decreases from the inlet to attain a minimum nearby the fin base surface and then increases again when going away the tube. For this case of calculation, the dew point temperature of air, corresponding to HR_i=50 % and $T_{a,i}$=27 °C, is equal to 16.1 °C, that is greater than the maximal temperature of the fin (13.4 °C) and the fin will be completely wet. The condensation factor C, defined by equation (64), allows us to verify this fact. Fig. 11 illustrates its distribution over the fin region.

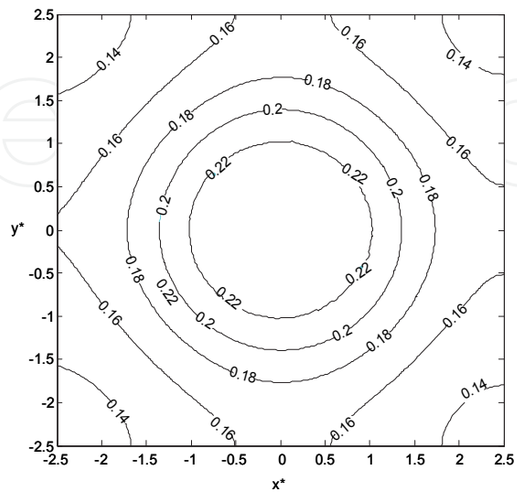

Fig. 11. Condensation factor distribution

As can be observed from Fig. 11, the condensation factor takes the largest values in the vicinity of the tube wall. The difference between the maximal and minimal values is about 30 %. The variation of C against the fin base temperature T_f and relative humidity HR can be demonstrated by the subsequent reasoning. The saturation humidity ratio of air may be approximated by a second order polynomial with respect to the temperature (Coney *et al.*, 1989, Chen, 1991):

$$W_S = a + bT + cT^2 \tag{68}$$

Where a,b and c are positives constants
The relative humidity has the following expression:

$$RH = \frac{P_v}{P_a - P_v} = \frac{W_a}{W_{S,a}} \times \frac{P_a - P_v}{P_a - P_{S,v}} \tag{69}$$

Where P_a, P_v and $P_{s,v}$ respectively represent, air total pressure, water vapor partial pressure and water vapor saturation pressure. If we neglect the water vapor partial and saturation pressures regarding the total pressure, then the following expressions of the absolute humidity arise:

$$W_a \approx RH \times W_{S,a} \tag{70}$$

$$W_{a,i} \approx RH \times W_{S,a,i} \tag{71}$$

Substituting equations (68) to (71) into the relation defining C (Eq. 64) yields:

$$C \approx RH \times \left[b + c\left(T_a + T_f\right) \right] - \left(1 - RH\right) \frac{a + bT_f + cT_f^2}{T_a - T_f} \tag{72}$$

The first and second order derivatives of the condensation factor with respect to the fin temperature can then be obtained readily from the previous equation:

$$\left.\frac{\partial C}{\partial T_f}\right|_{RH} = RH \times c - \left(1 - RH\right) \left[\frac{W_{S,a}}{\left(T_a - T_f\right)^2} - c \right] \tag{73}$$

$$\left.\frac{\partial^2 C}{\partial T_f^2}\right|_{RH} = -\left(1 - RH\right) \left[\frac{2W_{S,a}}{\left(T_a - T_f\right)^3} \right] \tag{74}$$

Obviously, for saturated air stream (RH=1), the first derivative of C takes the value of the constant c and is consequently positive. That demonstrates the increase of the condensation factor C with the fin temperature T_f. Conversely, for a sub-saturated air (RH<1), the second order derivative is always negative, that implies a permanent decrease of the condensation factor gradient with temperature. In this case, the critical point (maximum) for the function C(Tf) can be evaluated when $\left.\frac{\partial C}{\partial T_f}\right|_{RH} = 0$, thus, we obtain:

$$T_{f,cr} = T_a - \sqrt{(1-RH).W_{S,a} / c} \tag{75}$$

or

$$RH_{cr} = 1 - \frac{c\left(T_a - T_f\right)^2}{W_{S,a}} \tag{76}$$

Therefore the following statement is deduced:

- When $T_f > T_{f,cr}$ or $RH < RH_{cr}$, then $(\delta C/\delta T_f)_{RH} < 0$ and C decreases with T_f.
- When $T_f < T_{f,cr}$ or $RH > RH_{cr}$, then $(\delta C/\delta T_f)_{RH} > 0$ and C increases with T_f.

Fig. 11 is consistent with the above statement. Indeed, we can observe from Fig.10b and Fig.11 that the local condensation factor decreases with the fin temperature. Also, for the conditions in which the calculation related to Fig.10b and Fig.1 was performed, we get c=9.3458x10-6 and $W_{S,a}$=0.0202, hence, from Eqs. (75) and (76), $T_{f,cr}$=-6°C and RH_{cr}=90 %. Since Fig. 12 shows that $T_f > T_{f,b} > T_{f,cr}$, this observation validates our statement. However, it is also worth noting that the relative humidity of the moist air varies with the fin temperature and as a matter of fact, RH should be temperature dependent and the above statements hold along a constant relative humidity curve. Fig. 12 represents the distribution of air relative humidity in the fin region.

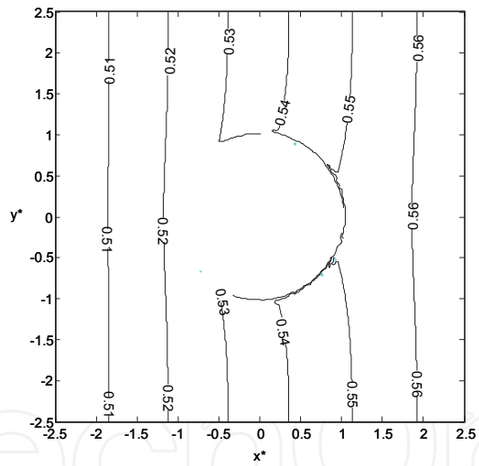

Fig. 12. Relative humidity distribution

As can be observed in Fig. 12, the relative humidity evolves almost linearly along the fin length. There is about 13 % difference between the inlet and outlet airflow. Correspondingly, the distribution of the condensate mass flux and the total heat flux density are carried out and illustrated in Fig. 13 and 14.

As the condensation factor takes place at the surrounding of the tube where the maximum gradient of humidity occurs, the condensate mass flux m''_c gets its maximal value at the fin base. Similarly, the maximal temperature gradient (T_a-T_f) arises at the fin base. That enhances the heat flow rate and a maximal value of q''_t is reached. However, these quantities decrease more and more along the dehumidification process due to the humidity and temperature gradients drop. Further results are shown in Fig.15, where the fin efficiency

curves are plotted. As the condensation factor C and the difference (T_a^* - T_f^*) grow around the tube, the fin efficiency will be maximal at the centre. As well, the quantities C and (T_a^* - T_f^*) are weaker at the upper and lower fin borders, that leads to the local reduction of the fin efficiency.

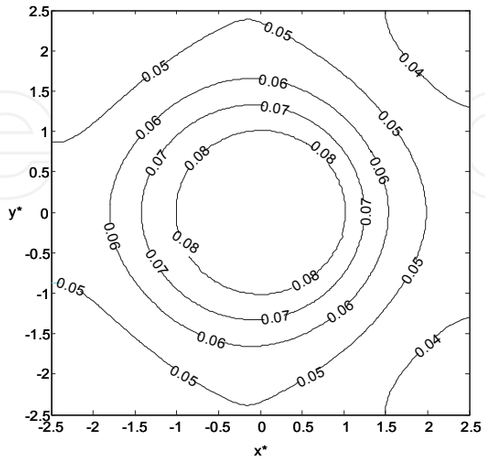

Fig. 13. Condensate mass flux distribution

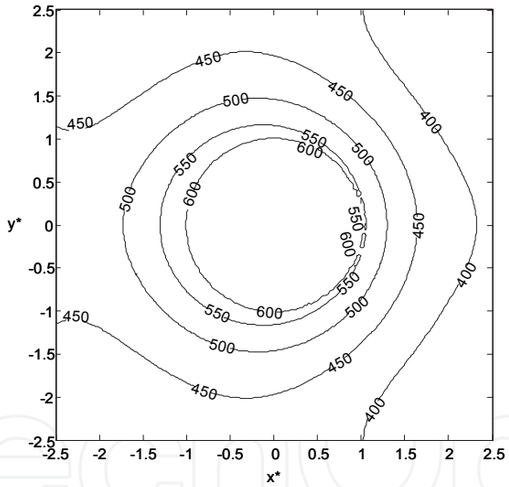

Fig. 14. Heat flux density distribution

3.2 The partially wet condition

The partially wet fin is obtained when the initial conditions are fixed to those of the central point (Table 1) except the inlet relative humidity which is settled to RH = 36 %, since $T_{f,b}<T_{dew,a}< T_{f,max}$. Condensation factor, relative humidity, total heat flux, and fin efficiency are estimated. The same general observations as those of the fully wet fin can be withdrawn. Condensation factor, total heat flux density and fin efficiency are maximal at the fin tube. However, the condensate droplets come to the end (C=0) from certain distance of the tube. At this point, the effect of some parameters, like inlet temperature, on the heat and mass transfer characteristics will be presented and discussed.

3.3 Effect of the inlet relative humidity

Both ideal and real fins are considered, and it is observed that δ_c starts to increase rapidly at about RH_i=40 %. For this case, the dry fin limit is estimated at RH_i=32 % and the fully wet condition beginning is estimated at RH_i=42 %. The order of magnitude of δ_c is about 0.1 mm, this value is comparable to that of Myers (1967) (0.127 mm) for, approximately, the same conditions. As δ_c increase with RH_i, the thermal resistance of the condensate increases and the heat transfer coefficient of the condensate α_c decreases (Eq.56). This agrees with the result of Coney et al. [10]. It was found also that the sensible heat transfer coefficient $\alpha_{sen,hum}$ is insensitive to RH_i (Fig. 21). Due to the smallness of the condensate film thickness, its thermal resistance ($1/\alpha_c$) is in the order of 0 to 5 % regarding the thermal resistance of the surrounding air. It is usually neglected. Conversely, the average overall heat transfer coefficient increases rapidly as the relative humidity increases. For a dry fin (RH_i<32 %), the total heat amount of both ideal and real fins is constant and consequently the fin efficiency remains constant in this range. The condensation appears from RHi=32 % for an ideal fin and from RH_i=36 % for a real fin. At this range (32%<RH_i<36%), the relative difference between ideal and real heats {($Q_{t,id}$-$Q_{t,r}$)/$Q_{i,id}$} is important, thus an abrupt decrease in fin efficiency is noticed. For RH_i=36 %, the condensation begins on the real fin and the total heat exchange rate $Q_{t,r}$ increases, thus the relative difference between ideal and real heats exchanges rates become less important and narrows more and more, therefore, the decrease in fin efficiency is gradual with a slop around 8 %. At RH_i=42 %, a complete wet condition is achieved for the real fin, the relative difference between $Q_{t,r}$ and $Q_{t,id}$ is almost constant. As well, the fin efficiency reduces slightly with a slop less than 4 %. Hence, the condensation, enhanced by increasing the relative humidity, can affect the efficiency and reduces it by 12 %. The fin efficiency gradient regarding relative humidity RH_i in the partial wet condition is more important than in the fully wet condition. The efficiency decreases more quickly in the partial wet condition. This result is similar of those of Rosario & Rahman (1999), Wu & Bong (1999), Liang *et al.* (2000), and Threlkeld (1970). However, Hong & Webb (1996), Elmahdy & Biggs (1983), and Mc Quiston (1975) have observed a more important decrease of the fin efficiency in the complete humidified phase (until 35 %). But, their models assume a constant temperature and relative humidity of the surrounding air. Kandlikar (1990) has re-examined the mathematical model of Elmahdy & Biggs (1983) and demonstrates that the fin efficiency in the fully wet condition should be insensitive to the relative humidity. It can be demonstrated that the results found by Hong & Webb (1996), and Mc Quiston (1975) are the consequence of the assumptions undertaken in their models. Indeed, if we consider again the expression of the fin efficiency in humid conditions (Eq. 67):

$$\eta_{f,hum} = \left(T_a^* - T_f^*\right)\frac{\left(1+\beta.C\right)}{\left(1+\beta.C_i\right)} \tag{77}$$

where;

$$\beta = \frac{Lv}{Le^{2/3}c_{p,a}} \quad \text{and} \quad C_i = \frac{W_{a,i} - W_{S,f,b}}{T_{a,i} - T_{f,b}}$$

Assuming Ta and C to be constant, as in the models of Hong & Webb (1996) and Mc Quiston (1975), the derivation of equation (77) with respect to RH_i yields:

$$\frac{\partial \eta_{f,hum}}{\partial RH_i} = -\frac{\partial T_f^*}{\partial RH_i} - \frac{\eta_{f,hum}.W_{S,a,i}.\beta}{\left(T_{a,i} - T_{f,b}\right)\left(1+\beta.C_i\right)} \tag{78}$$

Performing calculations of the fin efficiency derivative at $\eta_{f,hum}$=0.7 and using the parameters mentioned in figure 25, $T_{a,i}$=27 °C, $T_{f,b}$=9 °C, the following results yields:

$$-\frac{\partial T_f^*}{\partial RH_i} \approx 0.3 \; ; \; \frac{\partial \eta_{f,hum}}{\partial RH_i} \approx -1.1 \text{ for } RH_i=50\ \%$$

$$\text{and} \quad \frac{\partial \eta_{f,hum}}{\partial RH_i} \approx -0.42 \text{ for } RH_i=100\ \%$$

The decrease of the fin efficiency gradient between RH_i=50 % and RH_i=100 % is about 21 %. Therefore, the discordance founded between the different authors about the effect of the relative humidity on the fin efficiency may be the result of the models simplifications adopted.

3.4 Effect of the inlet air temperature

For a fixed RH_i, the increase of the inlet air temperature $T_{a,I}$ leads to increasing both fin and airflow temperatures (T_f and T_a). Thus, it has been noticed that the variations of the dimensionless fin and air temperatures are insignificant. However, the absolute moist air humidity raises and generates a more important humidity gradient between the fin wall and the surrounding air, and hence contributes to increase the condensation factor. Indeed, the derivation of C (Eq. 64) with respect to air temperature yields a positive derivative:

$$\left.\frac{\partial C}{\partial T_a}\right|_{RH} = c.RH + (1-RH).\frac{W_{S,f}}{T_a - T_f} > 0 \tag{79}$$

As the absolute humidity increase with $T_{a,I}$, the mass transfer is enhanced and the condensate-film thickness also increases. On the other hand, the increase of $W_{a,i}$ and W_a results in raising the condensation factor C and the latent heat rate, and that makes the overall heat transfer coefficient more important for a greater temperatures. Nonetheless, in the absence of condensation (RH_i from 0 to about 32 %), the overall and sensible heat transfer coefficients are equivalent and independent of the air temperature. With increasing air temperature, the total heat rate increases and the condensation starts for lower values of RH_i. The vapor condensation appearance is distinguished from RH_i=26 % (ideal fin) or RH_i=32 % (real fin) for $T_{a,i}$=30 °C and from RH_i=38 % (ideal fin) or RH_i=44 % (real fin) for $T_{a,i}$=24 °C. In the dry phase, the heat rate remains constant which implies a constancy of fin efficiency. At this stage, the fin efficiency decreases slightly with the increasing of air temperature. When condensation begins, the total heat rate increases with RHi and an abrupt decrease of fin efficiency is observed. This drop in the fin efficiency is slightly weak for greater air temperatures. In the fully wet condition and for higher relative humidity values, the fin efficiency decreases distinctly when Ta,I increase. These observations match with those reported by Kazeminejad (1995) and Rosario & Rahman (1999).

3.5 Effect of the fin base temperature

As stated above (Eq. 64), the dependence of C on the fin temperature T_f is marked with the existence of a critical value of RH_i where the trend progression is inverted. That is clearly

observed in Fig.30. For $RH_i<RH_{cr}$, the condensation factor decreases with the fin base temperature, whereas, for $RH_i>RH_{cr}$, C increases with $T_{f,b}$. Correspondingly, the trend of C is also inverted depending on whether the fin is real or ideal. Indeed, the ideal C factor is higher than the real C for $RH_i< RH_{cr}$, while it is lower for $RH_i> RH_{cr}$. As the absolute humidity near the fin wall $W_{S,f,b}$ increases with $T_{f,b}$, the amount of condensable vapor decreases, which in turn causes the reduction of the average condensate-film thickness as illustrated in Fig.31. However, the overall heat transfer coefficient follows the same trend as the condensation factor. For the dry condition, the sensible heat transfer is independent on $T_{f,b}$. Conversely, for the humid condition, $\alpha_{t,hum}$ decreases with $T_{f,b}$ when $RH_i< RH_{cr}$ and increases with Tf,b when $RH_i> RH_{cr}$. It is worth noting that since $\alpha_{t,hum}$ is influenced by the boundary layer thickness, the critical relative humidity RH_{cr} for which the trend of $\alpha_{t,hum}$ changes is to some extent different from the critical value obtained with C. In our case, $\alpha_{t,hum}$ begins to increase with $T_{f,b}$ from RH_i=85 % instead of RH_i=78 % as regards to C. The increase of $T_{f,b}$ leads an increase of $W_{S,f,b}$ and thus reduces both the total heat rate and the fin efficiency. In the partially humid condition case, a rapid drop of η_f is confirmed (about 10 %). This drop proves to be smaller for the fully wet condition (about 2%). Nevertheless, the variation of $T_{f,b}$ has no significant effect on the fin efficiency for the dry condition. Our results concerning the fin efficiency behavior with regard to the fin temperature agree with those of Rosario & Rahman (1999) but prove to be dissimilar from those established by Kazeminejad (1995). This is probably due to the fact that Rosario & Rahman consider the condensation factor to be variable while Kazeminejad assumes it as constant.

3.6 Effect of the inlet air speed

Increasing u_i reduces the hydro-thermal boundary layer thickness and increases the heat transfer coefficient. The temperature of air in the flow core also increases since the flow mass increases more rapidly than the heat flow rate, thus the fin temperature will be more important. Furthermore, as the air mass flow rate increases more rapidly than the condensate mass flow rate, the difference between airflow humidity and the saturated air humidity at the fin neighborhood (W_a – $W_{S,f}$) increases. That means an increase in the condensation factor as well as in the condensate thickness. In the same way, as the hydro-thermal boundary layer becomes finer for higher flow regime, the sensible heat transfer is favored. Thus, the sensible and overall heat transfer coefficients increase with u_i. However, this increase narrows down for highest air speed. On the other hand, the influence of u_i on the heat transfer is such as the total heat rate increase with increasing the flow regime. In the case of an ideal fin, the heat transfer increasing is quicker than for a real fin. This result has also been demonstrated numerically by Coney *et al.* (1989). Accounting for that effect, the fin efficiency should decrease with u_i, as mentioned in Fig. 36. Indeed, for lower velocities ui, the residence time of air is more important and the heat and mass transfer is more complete. This result is in adequacy with those of Liang *et al.* (2000) and Coney *et al.* (1989). Moreover, it is found that the difference between dry and humid fin efficiencies ($\eta_{f,dry}$ - $\eta_{f,hum}$) increases with u_i.

4. Conclusions

The present work proposes a two-dimensional model simulating the heat and mass transfer in a plate fin-and-tube heat exchanger. Ones the airflow profile was determined, the water vapor, air stream and fin heat and mass balance equations were solved simultaneously. It

was found that the overall heat transfer coefficient as well as the condensation factor increase with the inlet air temperature, the inlet relative humidity as well as the inlet velocity. Regarding the variations of $\alpha_{t,hum}$ and C with the fin base temperature, a critical value of relative humidity (RH_{cr}), corresponding to a minimum in $\alpha_{t,hum}$ and C was identified. This result still constitutes a point of discordance between many authors. The performed calculations of the wet-fin efficiency have demonstrated the decrease of $\eta_{f,hum}$ with increasing any of the parameters. However, a more important drop of $\eta_{f,hum}$ have been noticed for the partially wet condition. Moreover, the decrease of the fin efficiency with respect to the relative humidity and the fin base temperature, in the fully wet condition, is very weak especially for higher values of RH_i or $T_{f,b}$. The slope is quantified around 2 %.

5. References

Benelmir, R.; Mokraoui, S.; Souayed, A. (2009). Numerical analysis of filmwise condensation in a plate fin-and-tube heat exchanger in presence of non condensable gas, Heat and Mass Transfer Journal, 45, 1561–1573.

Chen, L.T. (1991). Two-dimensional fin efficiency with combined heat and mass transfer between water-wetted fin surface and moving moist airstreams, Int. J. Heat Fluid Flow, 12, 71-76.

Chen, H.T.; Song, J.P.; Wang, Y.T. (2005). Prediction of heat transfer coefficient on the fin inside one-tube plate finned-tube heat exchangers, Int. J. Heat Mass Transfer, 48, 2697-2707.

Chen, H.T. ; Wang, Y.T. (2008). Estimation of heat-transfer characteristics on a fin under wet conditions, Int. J. Heat Mass Transfer, 51, 2123-2138.

Chen, H.T.; Hsu, W.L. (2007). Estimation of heat transfer coefficient on the fin of annular-finned tube heat exchangers in natural convection for various fin spacings, Int. J. Heat Mass Transfer, 50, 1750-1761.

Chen, H.T.; Chou, J.C. (2007). Estimation of heat transfer coefficient on the vertical plate fin of finned-tube heat exchangers for various air speeds and fin spacings, Int. J. Heat Mass Transfer, 50, 47-57.

Choukairy, Kh. ; Bennacer, R. ; El Ganaoui, M. (2006). Transient behaviours inside a vertical cylindrical enclosure heated from the sidewalls, *Num. Heat Transfer (NHT*), 50-8, 773 – 785.

Coney, J.E.R. ; Sheppard, C.G.W. ; El-Shafei, E.A.M. (1989). Fin performance with condensation from humid air, Int. J. Heat Fluid Flow, 10, 224-231.

Elmahdy, A.H. ; Biggs, R.C. (1983). Efficiency of extended surfaces with simultaneous heat transfer and mass transfer, ASHRAE Journal, 89-1A, 135-143.

Hong, T.K. ; Webb, R.L. (1996). Calculation of fin efficiency for wet and dry fins, HVAC & Research, 2-1, 27-41.

Hsu, S.T. (1963). Enginnering heat transfer, D. VanNostrand Company, 240-252.

Johnson, R.W. (1998). The Handbook of Fluid Dynamics, Springer, USA.

Kandlikar, S.G. (1990). Thermal design theory for compact evaporators, Hemisphere Publishing, NY, pp. 245-286.

Kazeminejad, H. (1995). Analysis of one-dimensional fin assembly heat transfer with dehumidification, Int. J. of Heat mass transfer, 38-3, 455-462.

Khalfi, M.S. ; Benelmir, R. (2001). Experimental study of a cooling coil with wet surface conditions, Int. Journal of Thermal Sciences, 40, 42-51.

Lin, C.N.; Jang, J.Y. (2002). A two-dimensional fin efficiency analysis of combined heat and mass transfer in elliptic fins, Int. J. Heat Mass Transfer, 45, 3839-3847.

Lin, Y.T. ; Hsu, K.C. ; Chang, Y.J. ; Wang, C.C. (2001). Performance of rectangular fin in wet conditions: visualization and wet fin efficiency, ASME J. Heat Transfer, 123, 827-836.

Liang, S.Y.; Wong, T.N.; Nathan, G.K. (2000). Comparison of one-dimensional and two-dimensional models for wet-surface fin efficiency of a plate-fin-tube heat exchanger, Appl. Thermal Eng, 20, 941-962.

McQuiston, F.C. (1975). Fin efficiency with combined heat and mass transfer, ASHRAE Journal, 81, 350-355.

Myers, R.J. (1967). The effect of dehumidification on the air-side heat transfer coefficient for a finned-tube coil, Master Sc. Thesis, University of Minnesota.

Nusselt, W. (1916). Die Oberflachenkondensation des Wasserdampfes, Z. Ver. Dt. Ing, . 60, 541-575.

Rosario, L. ; Rahman, M.M. (1999). Analysis of heat transfer in a partially wet radial fin assembly during dehumidification, Int. J. Heat Fluid Flow, 20, 642-648.

Saboya, F.E.M. ; Sparrow, E.M. (1974). Local and average heat transfer coefficients for one-row plate fin and tube heat exchanger configurations, ASME J. Heat Transfer, 96, 265-272.

Threlkeld, J.L. (1970). Thermal Environmental Engineering, Prentice-Hall, New Jersey.

Wu, G. ; Bong, T.Y. (1994). Overall efficiency of a straight fin with combined heat and mass transfer, ASHRAE transactions, Part 1, 100, 367-374.

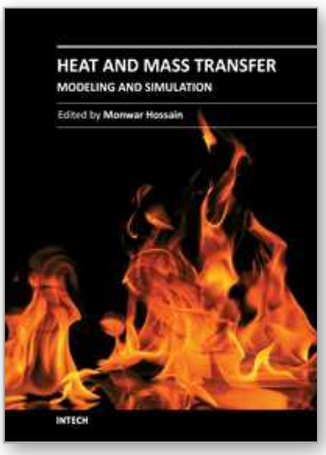

Heat and Mass Transfer - Modeling and Simulation

Edited by Prof. Md Monwar Hossain

ISBN 978-953-307-604-1
Hard cover, 216 pages
Publisher InTech
Published online 22, September, 2011
Published in print edition September, 2011

This book covers a number of topics in heat and mass transfer processes for a variety of industrial applications. The research papers provide advances in knowledge and design guidelines in terms of theory, mathematical modeling and experimental findings in multiple research areas relevant to many industrial processes and related equipment design. The design of equipment includes air heaters, cooling towers, chemical system vaporization, high temperature polymerization and hydrogen production by steam reforming. Nine chapters of the book will serve as an important reference for scientists and academics working in the research areas mentioned above, especially in the aspects of heat and mass transfer, analytical/numerical solutions and optimization of the processes.

InTech Europe
University Campus STeP Ri
Slavka Krautzeka 83/A
51000 Rijeka, Croatia
Phone: +385 (51) 770 447
Fax: +385 (51) 686 166
www.intechopen.com

InTech China
Unit 405, Office Block, Hotel Equatorial Shanghai
No.65, Yan An Road (West), Shanghai, 200040, China
中国上海市延安西路65号上海国际贵都大饭店办公楼405单元
Phone: +86-21-62489820
Fax: +86-21-62489821

IntechOpen